Scientia Iranica A (2021) 28(2), 666–681

SCIENTIA IRANICA

Sharif University of Technology
Scientia Iranica
Transactions A: Civil Engineering
http://scientiairanica.sharif.edu

Dispersion curves for media with lateral variation at different angles

M. Hashemi Jokar*, **H. Rahnema, and A. Baghlani**

Department of Civil and Environmental Engineering, Shiraz University of Technology, Shiraz, Iran.

Received 15 May 2019; received in revised form 7 September 2019; accepted 10 February 2020

KEYWORDS
Dispersion curves;
$f-k$ spectrum;
Lateral variation;
Phase velocity;
Surface wave method.

Abstract. The specification of soil surface layers is one of the most important parameters in civil engineering, geotechnics, and geophysics. The surface layer of the soil with lateral variation was modeled at different angles in finite element software. In each model, the shot was applied on two sides of the geophone array and the seismic wave data were recorded by geophones. Using the windowing methods of different lengths and moving along the array, the various geophone data were placed in different windows. Next, for each windowing, the frequency-wavenumber spectrum was obtained using the double Fourier transform, and then, the dispersion curve was plotted. In this regard, the variations in the resolution of the frequency-wavenumber spectrum and dispersion curve were investigated for different window lengths. The phase velocity changes due to the changes in the lateral variation angles were also investigated. For the media with lateral variation, the dispersion curves could be obtained along the array and the location of the start and end of lateral variation in the corresponding phase velocity range could be achieved with acceptable accuracy, and the estimated phase velocity could be used as initial velocities in the inversion and specification of soil surface layers.

1. Introduction

One of the most important parameters in the design of construction and geotechnical structures is determining the shear wave velocity of near-surface layers [1,2]. There are some variations in soil properties along the sides; these variations follow from the soil physical characteristics and should be considered in the design process. As a non-destructive method, the surface waves method has been used in recent years to determine the surface properties (soil layer properties in saturated or unsaturated condition such as density, shear velocity, shear strength, etc. [3–5]), and its use is increasingly growing [6].

In the layered media, the Surface Waves (SWs) have dispersive properties and the propagation velocity is a function of the frequency. It means that there is a certain phase velocity for each wavelength. The dispersion curves are obtained by plotting the frequency versus phase velocity [7]. Considering the fact that there is a variety of wavelengths in the generated wave, several modes of propagation can occur in the media. Therefore, the dispersion curve has several modes including the fundamental mode and higher modes. Among all these modes, the fundamental mode plays the most important role and can be considered as the dominant mode in the dispersion curve [8].

*. *Corresponding author.*
E-mail addresses: m.hashemijokar@sutech.ac.ir (M. Hashemi Jokar); rahnema@sutech.ac.ir (H. Rahnema); baghlani@sutech.ac.ir (A. Baghlani)

doi: 10.24200/sci.2021.53575.3313

One of the methods used to perform SWs testing is the Multichannel Analysis of Surface Waves (MASW) method. The seismic data recorded in the MASW method (traces) are in the time-space domain $(t-x)$. To obtain the dispersion curve, the double Fourier transform could be used, which transfers the data to the frequency-wavenumber $(f-k)$ domain. In this method, one Fourier transform is applied to transfer the data from the time domain (t) to the frequency domain (f). Another Fourier transform applies to transfer the data from the space domain (x) to the wavenumber domain (k). The frequency-wavenumber spectrum is obtained by plotting the data in the $f-k$ domain. Then, the k values corresponding to the maximum $f-k$ spectrum values could be obtained for different f values. The phase velocity (Vr) values are calculated by using the relationship between k, f, and Vr $(Vr = f/k)$, which ultimately, leads to plotting f versus Vr (dispersion curve) [7].

The lateral variation in the soil media causes the wave propagation and the phase velocity to be changed. Therefore, a more accurate calculation of the dispersion curve should be made. Considering the aforementioned description and the importance of lateral variation, Tian et al. (2003) [9] increased the spread length to increase the penetration depth of the SWs. They used the autojuggie on a dam by the MASW method with no lateral variation in the position of any Common Mid-Point (CMP). They were able to extract useful information using the body wave and SW data recorded at one time. Thus, they determined the near-surface shear wave velocity distribution with proper details.

Using the lateral variations of the Scholte-wave dispersion, Bohlen et al. (2004) [10] interpreted the 2D shear wave velocity for shallow-water marine sediments. The Scholte wave was created with an air gun towed behind a ship and recorded by receivers. Then, the wave field was determined by using a window along the receivers. They plotted the dispersion curves by the slowness-frequency spectrum method. Finally, the shear wave velocity profile was determined using the 1D inversion for the center of each window.

Using the CMP cross-correlation, Hayashi and Suzuki (2004) [11] collected data from multi-channel and multi-shot SWs and obtained the dispersion curves. They performed data processing with the Common Depth-Point (CDP) analysis with 2D seismic reflection survey data. Using the MASW method, they determined the dispersion curve for CMP cross-correlations and obtained the profiles of shear wave velocity.

Luo et al. (2008) [12] performed the horizontal resolution analysis for a pair of synthetic traces and found the following results: 1) For the receivers of lower distance, the more evident shear wave velocity was achieved, whereas the relative error was found to be larger, 2) The phase velocities at higher frequencies have less relative error than the phase velocities at lower frequencies, and 3) The signal-to-noise ratio of the data is very influential on the relative error of the inverted S-wave velocity. Therefore, they were able to make a good trade-off between the receiver spacing and the accuracy of the shear wave velocity profile.

Socco et al. (2009) [13] used a moving window along the receivers and obtained the dispersion curve. They successfully used the laterally constrained inversion applied in the optimization for the Monte Carlo algorithm to determine the pseudo-2D shear wave velocity for the synthetic and real data.

Vignoli and Cassiani (2010) [14] used the phase-offset slope changes (knee-point) method to determine the shear wave velocity using 1D inversion applied to the separated sections. They also just provided acceptable results for the media with lateral variation with the 1D fundamental-mode inversion. Furthermore, they concluded that the higher-modes data with some extra information could be further used in the inversion process depending on the desired level of accuracy.

According to the multi-aspect method, the propagation of the guided wave in the viscoelastic plate affected by the viscoelasticity was investigated by Othmani et al. (2016) [15]. They proposed a Legendre polynomial method to formulate the guided waves equation and validated it with available data. They noticed that the viscoelastic models affect the attenuation curves and do not affect the dispersion curves.

Othmani et al. (2017) [16] studied the lamb wave propagation through a sandwich plate and discussed the convergence and accuracy of a Legendre polynomial series. They developed the influences of the volume fraction p and thickness h_{FGPM} of the Functionally Graded Piezoelectric Materials (FGPM) middle layer on the lamb dispersion curves. They found that at a given frequency range, as the volume fraction p increases, the number of modes decreases, and the phase velocity increases.

Othmani et al. (2018) [17] modeled the guided dispersion curves solutions in anisotropic fiber-reinforced composite media using a Legendre polynomial approach with high computational efficiency and simplicity. They analyzed the reductions in the material properties influence on the fundamental guided wave dispersion curves. As illustrated in the previous researches, lamb wave dispersion curve was studied by Othmani et al. (2016), Othmani et al. (2017), and Othmani et al. (2017) [15–17]. This paper investigates the Rayleigh waves dispersion curve in the media with a lateral variation.

Hashemi Jokar et al. (2019) [18] detected subsoil lateral heterogeneities using multi-offset phase analysis of SW data. They reproduced synthetic modeling seismograms that were consistent with the recorded data at a vertical and lateral heterogeneities industrial site. So, they defined heterogeneities in complex environments and showed that the multi-offset phase analysis could be used even at a very small spatial scale.

In all previous studies, the slope effect of lateral variation has not been studied. In most of them, the lateral variation has been vertical, and the effect of other angles was less considered. In this study, the finite element method is used to create lateral variation soil models of angles 10 to 170 degrees with 20-degree increments which are located in the half-space. In these models, the active shot is introduced on two sides of the model (loose and moderate soil) and data are recorded. Then, using the $f-k$ method, the dispersion curves are plotted. The following is a more detailed description of modeling and data analysis.

2. Materials and method

In recent years, the finite element method has been successfully used to solve dynamic and seismic problems [8,18–22] . In the finite element method, the media is divided into some finite elements. The general equation of motion can be defined by considering the strain-displacement relations, the material constitutive relations, and the equilibrium equations as:

$$M\ddot{u}+C\dot{u}+Ku=f, \tag{1}$$

where M, C, and K are mass matrix, damping matrix, and stiffness matrix, respectively, u, $\dot{u}$ and $\ddot{u}$ are the displacement vector and its time derivatives, respectively and f is the vector of applied loads.

To calculate the dispersion curve, the damping matrix can be neglected, so, the displacements and forces in the element's node can be written as:

$$u=Ue^{i\omega t}, \tag{2}$$

$$f=Fe^{i\omega t}, \tag{3}$$

where $i=\sqrt{-1}$, ω is the angular frequency and t is the time. Therefore, Eq. (1) can be rewritten as follows:

$$\left[K-\omega^2 M\right]U=F, \tag{4}$$

where:

$$U=\begin{bmatrix}U_1^T & U_2^T & U_3^T & U_4^T\end{bmatrix}^T, \tag{5}$$

$$F=\begin{bmatrix}F_1^T & F_2^T & F_3^T & F_4^T\end{bmatrix}^T, \tag{6}$$

where U_i and F_i are nodal displacements and forces, respectively, for four nodes ($i=1-4$). Considering the Bloch boundary conditions [23], U can be defined as follows:

$$U_2=U_1e^{ik_xa},\quad U_3=U_1e^{ik_yb},\quad U_4=U_1e^{i(k_xa+k_yb)}, \tag{7}$$

where k_x and k_y are the wavenumbers along the x and y direction, respectively, a and b are unit cell lengths along the x and y direction, respectively. Then:

$$U=\begin{bmatrix}I & e^{ik_xa}I & e^{ik_yb}I & e^{i(k_xa+k_yb)}I\end{bmatrix}^T\quad U_1=B_1U_1, \tag{8}$$

$$B_1=\begin{bmatrix}I & e^{ik_xa}I & e^{ik_yb}I & e^{i(k_xa+k_yb)}I\end{bmatrix}^T. \tag{9}$$

In node 1, the equilibrium equation can be presented as follows:

$$\begin{bmatrix}I & e^{-ik_xa}I & e^{-ik_yb}I & e^{-i(k_xa+k_yb)}I\end{bmatrix}\quad F=B_2F=0, \tag{10}$$

$$B_2=\begin{bmatrix}I & e^{-ik_xa}I & e^{-ik_yb}I & e^{-i(k_xa+k_yb)}I\end{bmatrix}. \tag{11}$$

Therefore, Eq. (4) can be presented as follows:

$$\left[B_2KB_1-\omega^2B_2MB_1\right]U_1=0, \tag{12}$$

Eq. (12) is the wave propagation eigenvalue problem. Using the finite element method, Eq. (12) can be solved the wave propagation in the media and get the dispersion curve . ABAQUS [24] is a powerful software based on the finite element that has been used with acceptable accuracy to model various problems, especially SWs [8,18–20,25,26]. In geophysical testing, such as the SWs test, the resultant strains are generally so small that the soil behaves like a linear elastic material, adequately justifying the use of a linear stress-strain relationship. In this regard, elastic parameters of the soil were used for simulating the SWs in ABAQUS. Properties of the soil layers that should be defined in the ABAQUS simulation are compressional wave velocity (V_P), shear wave velocity (V_S), density (ρ), Young's modulus (E, see Eq. (13), and Poisson ratio (μ, see Eq. (14)) [8]:

$$E=\frac{\rho {V_s}^2\left(3{V_P}^2-4{V_S}^2\right)}{{V_P}^2-{V_S}^2}, \tag{13}$$

$$\mu=\frac{{V_P}^2-2{V_S}^2}{2\left({V_P}^2-{V_S}^2\right)}. \tag{14}$$

In the different steps of SW modeling with ABAQUS software, some special points should be considered. In the following, these steps and their solutions are outlined:

1. Absorbing boundaries: For determining the boundaries of the model, it should be noted that the return of the wave to the model should be prevented, because , in reality, there will be no return from the half-space to the model and the wave on its path

propagated towards infinity. Therefore, this should be applied in software so that the unnecessary large-scale modeling could be avoided. One method of boundary modeling is using the Absorbing Layer with the Increased Damping (ALID) method. The ALID method consists of several layers (more than 10 layers) with a specific thickness (usually one meter) where the characteristics of the layers are the same as their adjacent media, with the difference that as these layers move away from the model, their damping is increased. The damping used in ALID is the Rayleigh damping coefficients. The Rayleigh damping, $[C_R]$, is defined as:

$$[C_R] = C_M [M] + C_K [K], \tag{15}$$

where $[M]$ and $[K]$ are mass and stiffness matrices, respectively, and C_M and C_K are mass and stiffness damping coefficients, respectively. Due to the sensitivity involved in solving the dynamic problems, C_K requires loading with very small time intervals, which increases the time and cost of the problem solving; thus, it is recommended that $C_K = 0$ be considered [8]. The values used for C_M in Table 1 are provided for 10 ALID layers. As can be seen, these coefficients are increasing as multiplied by two for each region, and this increase must be as much as that it does not cause a significant change in the damping between the two layers of the ALID and, consequently, the return of the wave at the boundary of the two layers;

2. Pulse force: The pulse force used to generate SWs should be applied to provide the frequency content required for penetration in all layers. Therefore, a pulsed force is used in the form of a rectangular load of 40 μs duration, which contains the frequency content between 5 and 100 Hz [20];
3. Mesh type and mesh size: The 4-node bilinear plane strain quadrilateral mesh type was used to mesh the models. To get an accurate mode shape, it is better to have the mesh size smaller than 1/3 to 1/5 of the wavelength [27,28]. So, the mesh size should be obtained in proportion to the minimum wavelength, i.e. dx. The mesh sizes ranging between dx/7 and dx/9 (i.e. 6 to 8 nodes per minimum wavelength, respectively) led to acceptable accuracy along with reasonable processing time. So, the mesh size was adjusted to dx/8 [8];
4. Time increment size: The ABAQUS dynamic explicit time integration method was used to solve the model. Furthermore, the Courant-Friedrichs-Lewy (CFL) condition demands that the propagating wave should not travel by more than one element size during a time step. Therefore, to overcome the computational stability limitation, the time increment size was set to 0.0125 ms, and the model was run [8];
5. Interface between materials: To make the interface between the different materials, the sketch partition method was used. This method allows different parts with different materials to be separated and causes the elements (the bilinear plane strain quadrilateral which is used in the whole model) in the interface to have the same common nodes and connect them as well.

3. Synthetic modelling validation

Hashemi Jokar et al. (2019) [18] experimental data was used to validate the synthetic models. To generate the synthetic model, the L4 acquisition line, presented in the study of Hashemi Jokar et al. (2019) [18], was chosen and the dispersion curve for both data set was calculated. Also, to avoid the model geometry complexity, the southern part of line L4, which includes a lateral variation between two different materials (from the distance 48 to 144 m), was modeled. The model geometry and the material properties of the L4 acquisition site are presented in Figure 1 and Table 2, respectively. The L4 acquisition [18] synthetic model geometry with the ALIDs are shown in Figure 2.

For the experimental [18] and synthetic data, the traces and the dispersion curve images are presented in Figure 3 and the dispersion curves are presented in Figure 4. To obtain the difference between the dispersion

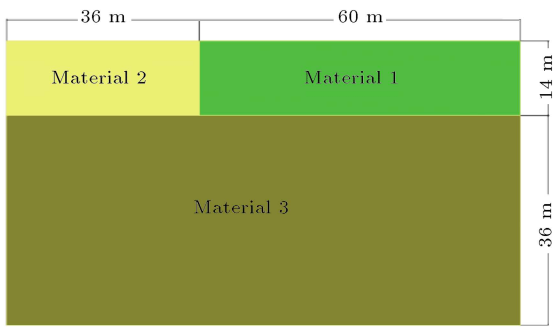

Figure 1. Model geometry of the L4 acquisition site in [18].

Table 1. Damping coefficient of mass inside the model and Absorbing Layer with the Increased Damping (ALID) layers.

ALID region	Inside model	1	2	3	4	5	6	7	8	9	10
C_M	2.5	4	8	16	32	64	128	256	512	1024	2048

Table 2. Material properties of the L4 acquisition [18].

Material	Material type	Poisson ratio	Density (kg/m^3)	Young's modulus (kN/m^2)	Compressional wave velocity (m/s)	Shear wave velocity (m/s)
Material 1	Continental silty-clay	0.32	1700	179736	390	200
Material 2	Marine clay	0.29	1600	59362	220	120
Material 3	Flysch rock	0.32	1900	16254300	3500	1800

curves for the experimental [18] and synthetic data, the Root-Mean-Square Error (RMSE) [4] is calculated as follows:

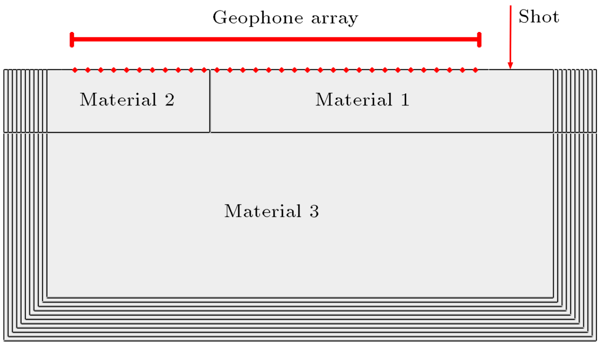

Figure 2. Synthetic model geometry for validation (generated according to the L4 acquisition line in [18]).

$$RMSE = \sqrt{\frac{\sum_{i=1}^{n} (V_{phE} - V_{phS})^2}{n}}, \tag{16}$$

where V_{phE} and V_{phS} are the experimental and synthetic phase velocities, respectively and n is the number of phase velocities in the dispersion curves.

The RMSE value for the experimental [18] and synthetic data phase velocities is equal to 15.153 m/s. As can be seen in Figure 4 and considering the RMSE value, there is a good agreement between the dispersion curve for the experimental and synthetic data. Also, both dispersion curves asymptote to Material 1 phase velocity and their fundamental mode is visible at a very high resolution. Therefore, the synthetic models can be successfully used in the SW propagation through the media with a lateral variation.

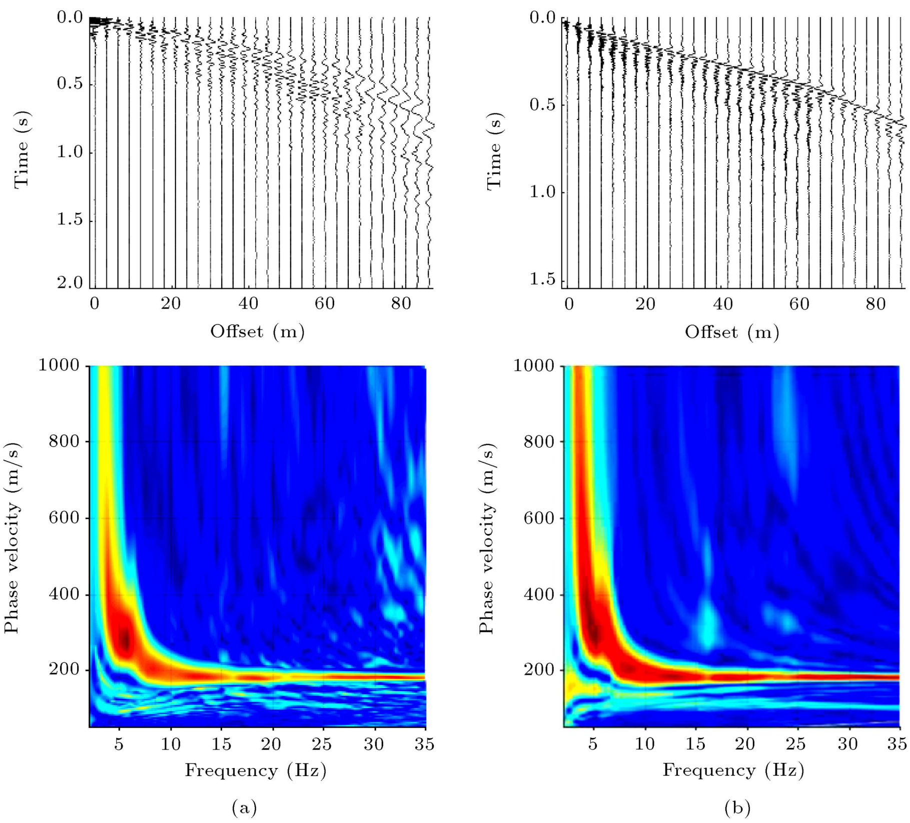

Figure 3. Traces and dispersion curve images for (a) experimental data [18] and (b) synthetic model data.

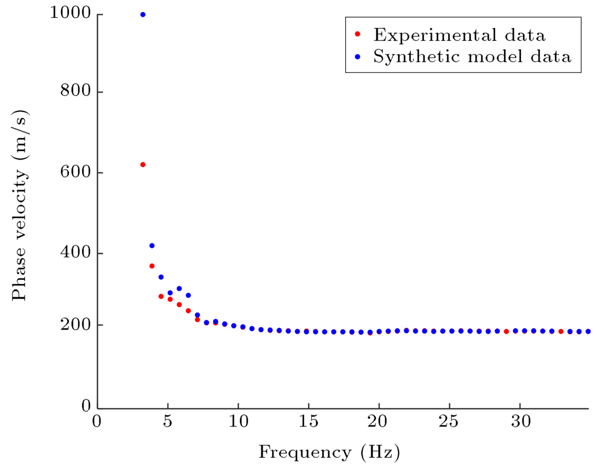

Figure 4. The dispersion curves for the experimental [24] and synthetic data.

4. Numerical modeling and results

The numerical modeling in ABAQUS software is a 2D single-layer soil on the half-space models in which the first layer has inclined lateral variations. The model of lateral variations with angle α is presented in Figure 5. In this regard, different angles for the lateral variation model were considered as 10, 30, 50, 70, 90, 110, 130, 150, and 170 degrees. Table 3 presents the modeled soil characteristics. As seen in this table, three soil types are used for modeling: loose, moderate, and hard soil. Also, by applying the shot on two sides of the model, two types of solutions could be achieved, including:

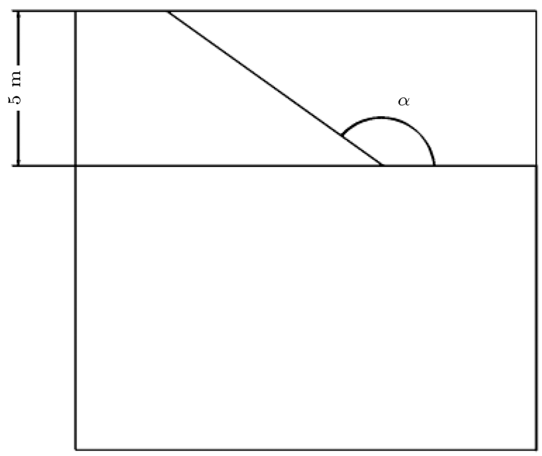

Figure 5. Model of lateral variations with angle α.

1) According to the soil side, the sledgehammer shot is introduced (on the loose or moderate soil), 2) The SWs propagate from the loose to the moderate soil or vice versa. Therefore, there are 18 models with 9 different angles (9 models for the shot on loose soil and 9 models for the shot on moderate soil). To analyze the data and obtain the dispersion curves, the frequency-wavenumber spectrum method was used. For this purpose, the windows of different array lengths (12, 24, 36, 48, 60, 72, 84, 96, 108, and 120 traces) were used to move along the array which incorporate different traces. Then, by choosing the maximum value for the frequency-wavenumber spectrum, the dispersion curve could be achieved for each window. In the following, the modeling results are presented for both shot modes.

4.1. Shots on loose soil

Soil models were modeled with lateral variations at different angles and shot on loose soil (Figure 6). In Figure 6, there are two vertical lines indicating the start (L I) and the end (L II) of the inclined slope. The SW data were gathered for all models. Figure 7 presents the traces taken for the model with a shot on the loose soil and lateral variations of angles 10, 90 and 170 degrees and the L I and L II lines (presented in Figure 6). As can be seen, the location of lateral variations on the ground surface is evident in the traces.

In the following, the frequency-wavenumber spectra are provided for the array lengths of 120 traces (one window including traces 1–120) and only for angles 10, 90, and 170, in Figure 8, for brevity. After obtaining the frequency-wavenumber spectra for

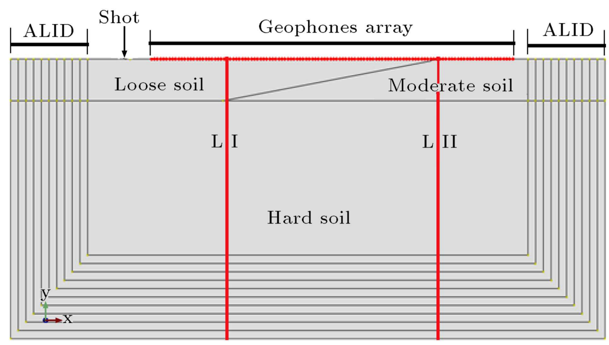

Figure 6. Model of lateral variations with 10-degree angle and shot on loose soil (two vertical lines (L I and L II) indicating the start and the end of the inclined slope).

Table 3. Properties of soil used in ABAQUS modeling.

Soil type	Shear wave velocity (m/s)	Compressional wave velocity (m/s)	Young's modulus (kN/m^2)	Density (kg/m^3)	Poisson ratio
Loose	100	200	50667	1900	0.333
Moderate	200	400	202667	1900	0.333
Hard	300	600	456000	1900	0.333

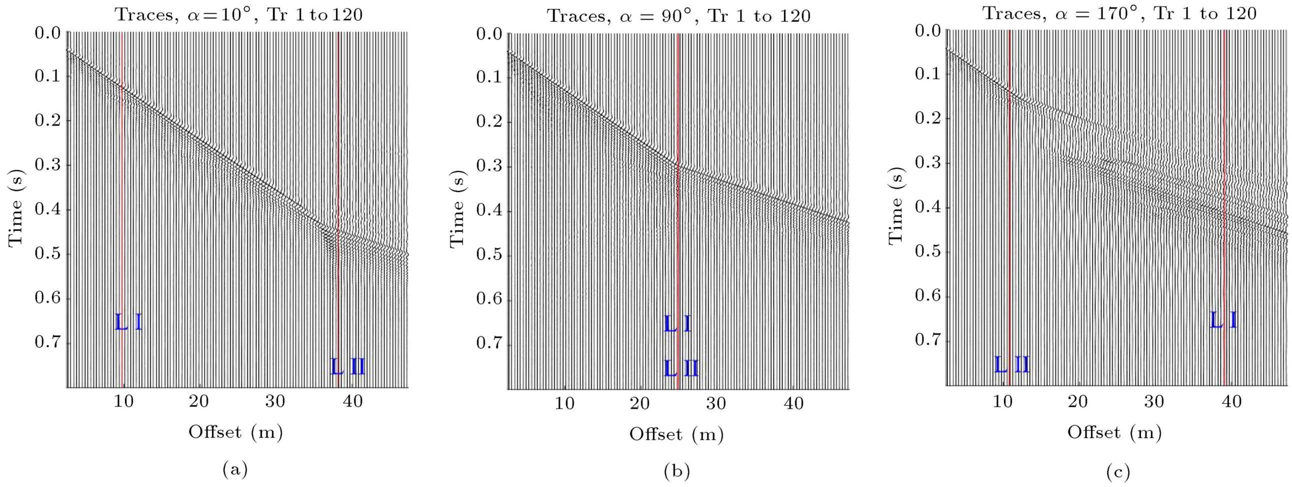

Figure 7. Traces taken for the model with a shot on loose soil and lateral variations at angles 10, 90, and 170 degrees (two vertical lines (L I and L II) indicating the start and the end of the inclined slope (see Figure 6)).

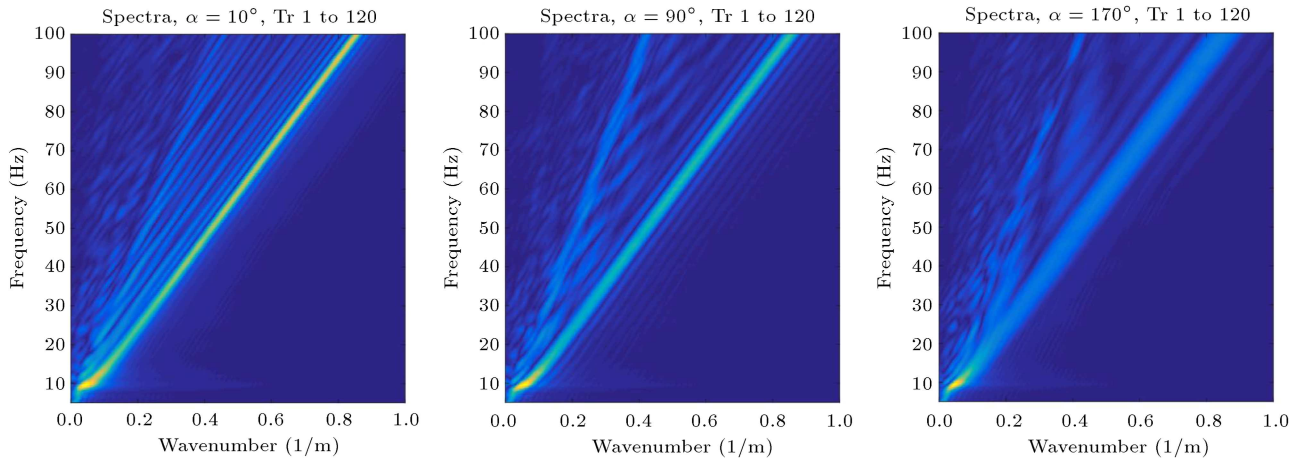

Figure 8. Frequency-wavenumber spectra for the model with a shot on loose soil at angles 10, 90, and 170 and window lengths of 120 traces.

different windowing, the maximum values for each spectrum were selected and the dispersion curve was obtained. Figure 9 presents the dispersion curves of the models with a shot on loose soil and different lateral variation angles for the window length of 12, 60, and 120 traces. As seen in Figure 9(a), for the window length of 12 traces, there is no change in the dispersion curve for traces 1–12 at different angles, because the lateral variations are still not introduced for the desired window. But in the traces 55–66, which are located just above the center of the lateral variations, the dispersion curves vary for different angles and the velocity at high frequencies is asymptotic proportional to the Rayleigh wave velocity of the soil located on the ground surface. However, in the traces 109–120 where the window is located after lateral variations, some fluctuations are observed in the dispersion curve around the phase velocity of the moderate soil, which is due to passing through the lateral variations at different angles that affect the wave field.

As seen in Figure 9(b), for traces 1–60, some slight variations are observed at low frequencies for different angles, which is because this window only covers half of the lateral variations and is not much affected. For the traces 31–90 in the center of lateral variation, low frequencies have relatively large variations in the dispersion curve for lateral variations at different angles, but the dispersion curve at high frequencies for all angles, except for 170-degree angle that is asymptotic to phase velocity of the moderate soil, is asymptotic to the phase velocity of the loose soil. And in the case of traces 61–120, for models with lateral variations at different angles, there are many variations in the dispersion curve at low frequencies, and all these curves, except the model with 10-degree lateral variations that is asymptotic to the phase velocity of

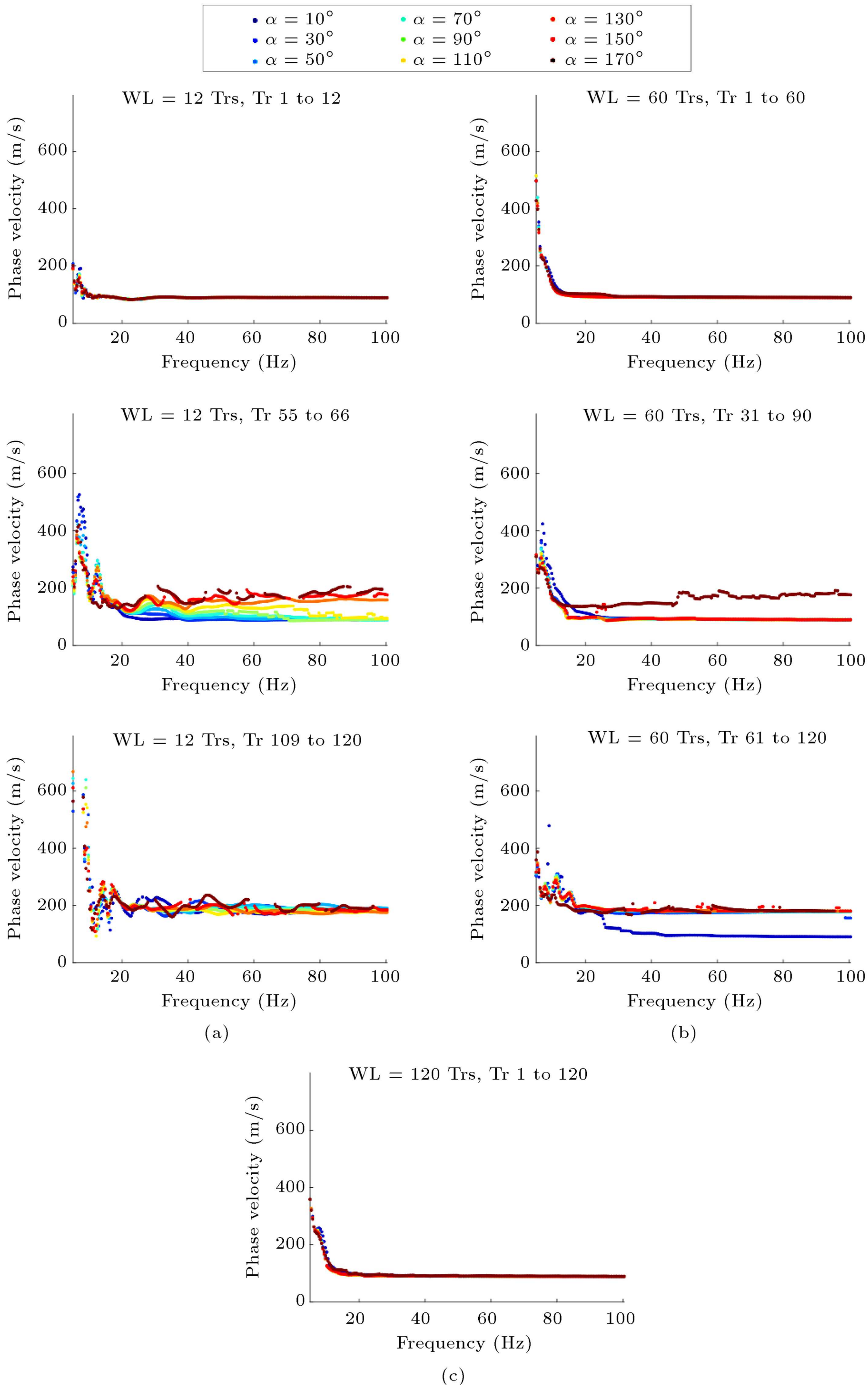

Figure 9. Dispersion curves of models with a shot on loose soil at different angles of lateral variation for window length of (a) 12 traces, traces 1–12, 55–66 and 109–120, (b) 60 traces, traces 1–60, 31–90 and 61–120, and (c) 120 traces, traces 1–120.

the loose soil, is asymptotic to the phase velocity of the moderate soil with a slight fluctuation.

As shown in Figure 9(c) for the traces 1–120, some slight variations are observed at the low frequencies for the dispersion curves of models with different angles, but all of these curves are asymptotic to the phase velocity of the loose soil. This is because the window is large enough to present the overall behavior of the wave passing from the medium with different angles of lateral variations,(also known as the lateral variation region) and the media before and after it.

As can be seen from Figure 10, the dispersion

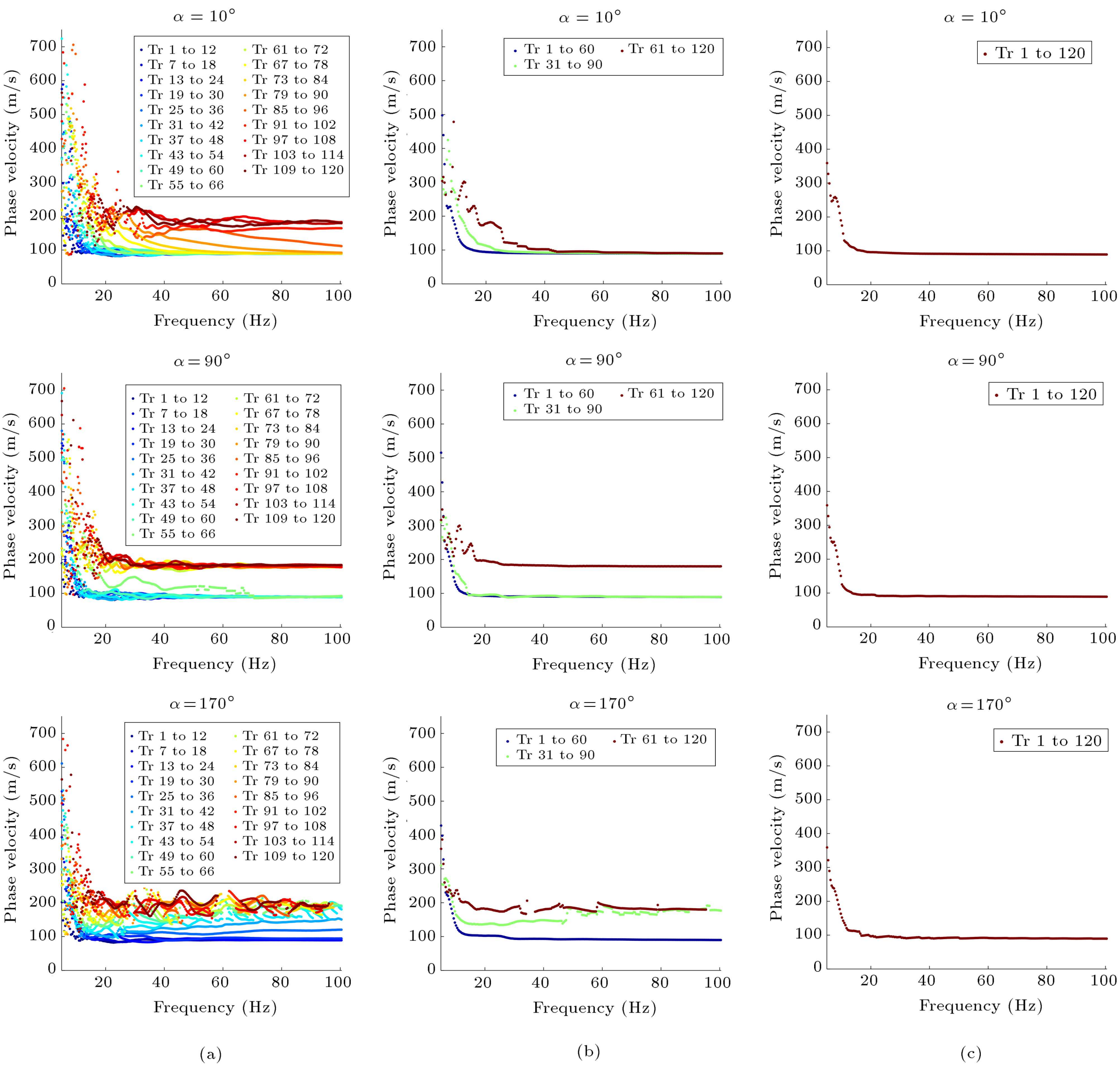

Figure 10. Dispersion curves of the model with a shot on loose soil and lateral variation of angles 10, 90, and 170 degrees and window length of (a) 12 traces, (b) 60 traces, and (c) 120 traces.

curves of the model are presented for a shot on the loose soil and lateral variation angles of 10, 90, and 170 degrees and window lengths of 12, 60, and 120 traces. In Figure 10(a), by moving the window along the array, the dispersion curves are asymptotic from the phase velocity of the loose soil to the phase velocity of the moderate soil at high frequencies. However, in Figure 10(b), for the lateral variation model with a 10-degree angle, the dispersion curves are asymptotic to the phase velocity of loose soil. But in the 90 and 170-degree modes, the dispersion curves become asymptomatic to the loose or moderate soil depending on the position of the window. Figure 10(c) is the same as Figure 9(c) illustrating the dispersion curves for the angles 10, 90, and 170 degrees separately and the relevant descriptions are presented in the preceding paragraph.

4.2. Shots on moderate soil

The layered media with lateral variations were modeled at different angles with a shot location on the moderate soil (Figure 11). In Figure 11, there are two vertical lines indicating the start (L I) and the end (L II) of the inclined slope. Figure 12 presents the traces taken for the model with a shot on the moderate soil and the lateral variations of angles 10, 90, and 170 degrees and, the L I and L II lines (presented in Figure 11). As seen in the figure, the slope of waves travel path

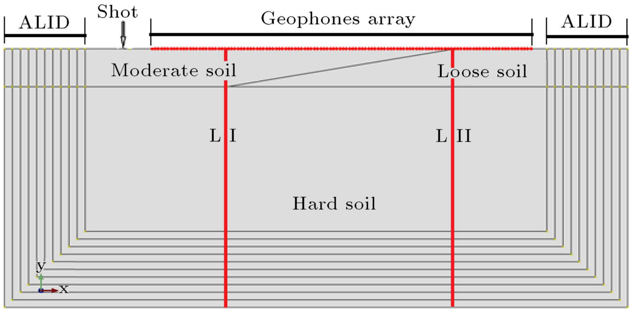

Figure 11. Model of lateral variations with 10-degree angle and shot on moderate soil (two vertical lines (L I and L II) indicating the start and the end of the inclined slope).

in the traces change at the outcrop of lateral variation (the location of the intersection of the lateral variation interface line with the ground surface) and the wave travel path for the traces located in the moderate soil is more horizontal than the wave travel path for traces located in the loose soil. This is because the velocity in the moderate soil is higher than that of the loose soil, and the wave in the moderate soil travels more distance than that of the loose soil in less time.

Figure 13 presents the dispersion curves of the model with a shot on the moderate soil and the various angles of lateral variation for the window length of 12, 60, and 120 traces. As seen in Figure 13(a), for the window length of 12 traces, for traces 1–12, the dispersion curve of all models at the high frequencies is asymptotic to the phase velocity of the moderate soil and no change was observed. But for the traces 55–66, by changing the angle of the lateral variations from 10 to 170 degrees, the phase velocity of the dispersion curves at high frequencies changes from the phase velocity of the moderate soil to that of the loose soil. And for traces 109–120, the phase velocity of all models is asymptotic at different angles of lateral variations and at high frequencies to the phase velocity of loose soil with a slight fluctuation. In Figure 13(b), for the traces 1–60, only for the model with the lateral variation angle of 170 degrees, the dispersion curve is asymptotic to the phase velocity of the loose soil, and the rest of the models become asymptotic to the phase velocity of moderate soil. For the traces 31–90, for models with lateral variations of less and more than 90 degrees, the dispersion curves at the high frequencies are asymptotic to the phase velocity of loose and moderate soils, respectively. For traces 61–120, all models are also asymptotic to the phase velocity of loose soil. Regarding Figure 13(c), for small and large-angle lateral variation models, the dispersion curves at high frequencies are asymptotic to the phase velocity of moderate and loose soils, respectively. This is because the traces 1–120 provide the overall behavior of the wave throughout the layout, which is located at the small angles of the moderate soil over the more length near the ground surface and at the large angles of loose soil near the ground surface, causing it to become asymptotic to the phase velocity of the soil with more length near the ground surface.

The dispersion curves of the models are presented in Figure 14 with a shot on the loose soil and lateral variation angles of 10, 90, and 170 degrees and window length of 12, 60, and 120 traces. In Figure 14(a), by moving the window along the array, the dispersion curves are asymptotic from the phase velocity of the moderate soil to the phase velocity of the loose soil at high frequencies. But in Figure 14(b), for a model with lateral variations of 10 and 90 degrees, the dispersion curves are asymptotic to the phase velocity of loose or moderate soils depending on the position of the window, but for the model with lateral variations of 170 degrees, the dispersion curves become asymptotic to the

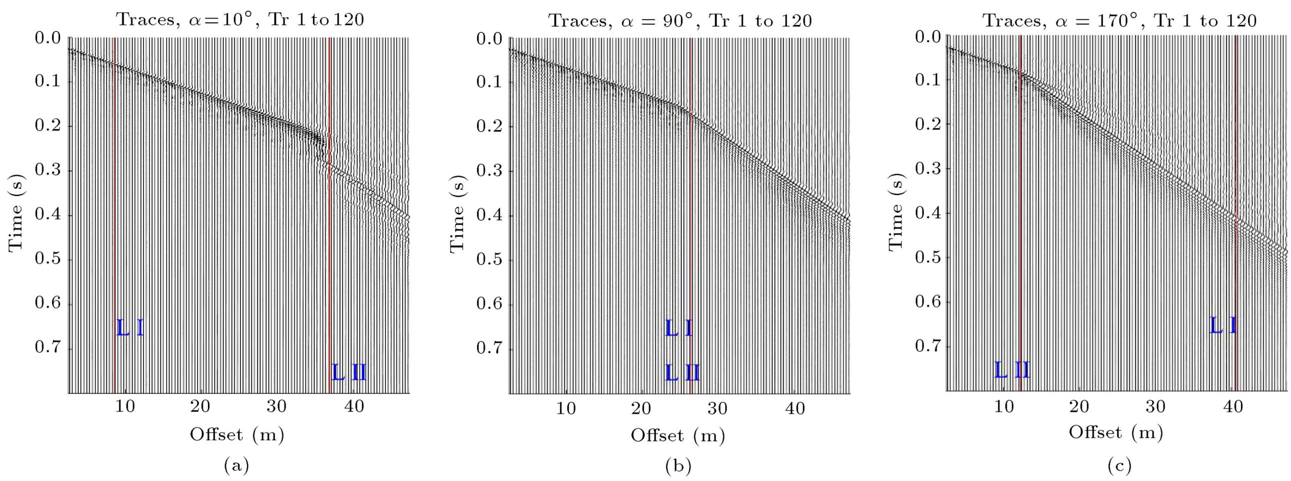

Figure 12. Traces taken for the model with a shot on moderate soil and lateral variations at angles 10, 90 and 170 degrees (two vertical lines (L I and L II) indicating the start and the end of the inclined slope (see Figure 11)).

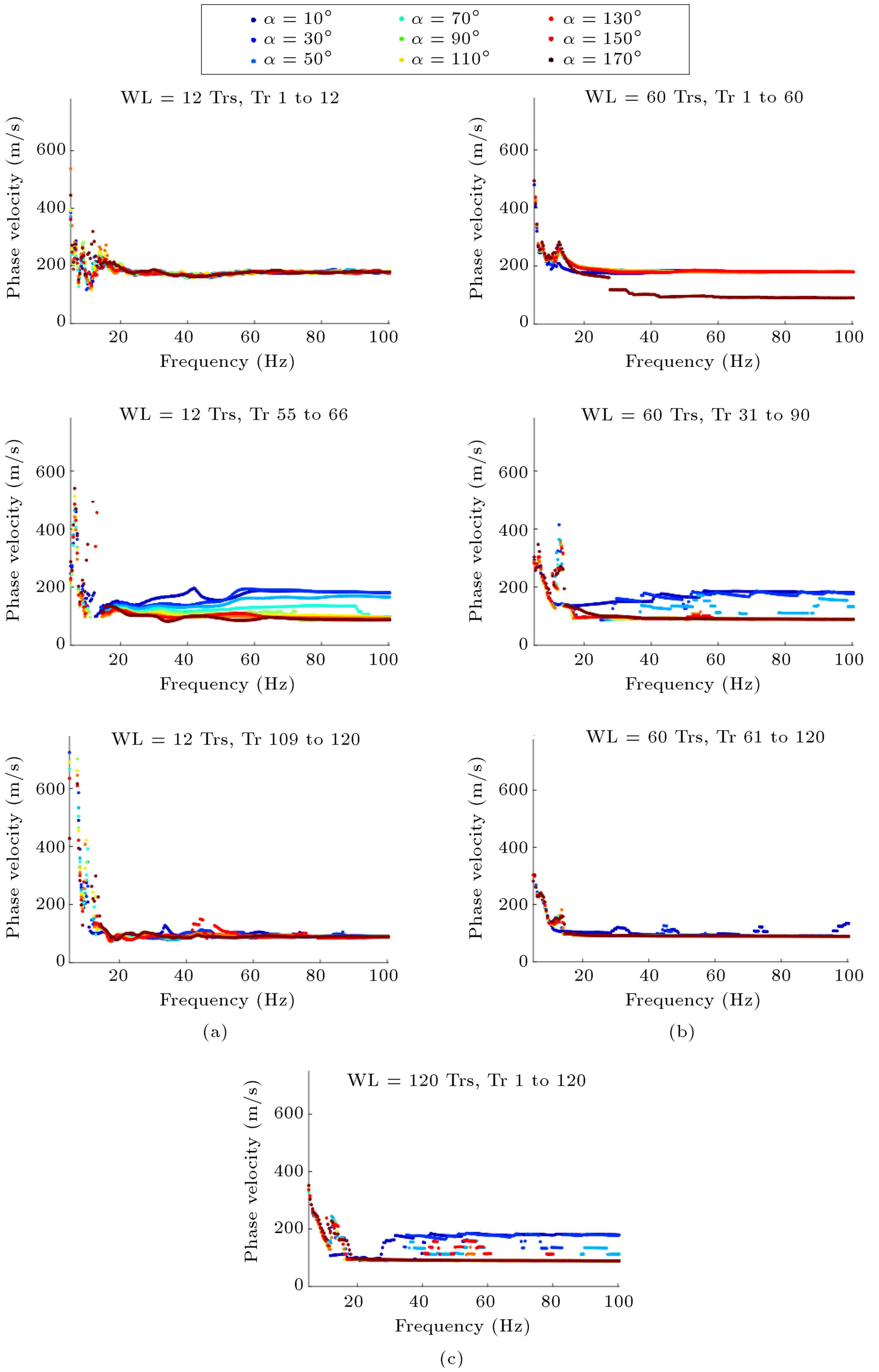

Figure 13. Dispersion curves of models with a shot on moderate soil at different angles of lateral variation for window length of (a) 12 traces, traces 1–12, 55–66 and 109-120, (b) 60 traces, traces 1–60, 31–90 and 61–120, and (c) 120 traces, traces 1–120.

phase velocity of loose soil. Figure 14(c) is the same as Figure 13(c), with the dispersion curves are separately plotted for 10, 90, and 170 degrees, and the relevant descriptions are presented in the preceding paragraph.

4.3. Model with reverse velocities

In the following, the models with reverse velocity (velocity decreases with depth) are generated (Figure 15). Figure 16 and Figure 17 present the dispersion curves of the model with a shot on the moderate and hard soil, respectively, and the various angles of 10, 90 and 170 degrees (for the sake of brevity), lateral variation for the window length of 12, 60, and 120 traces. As it can be seen in these figures, lateral

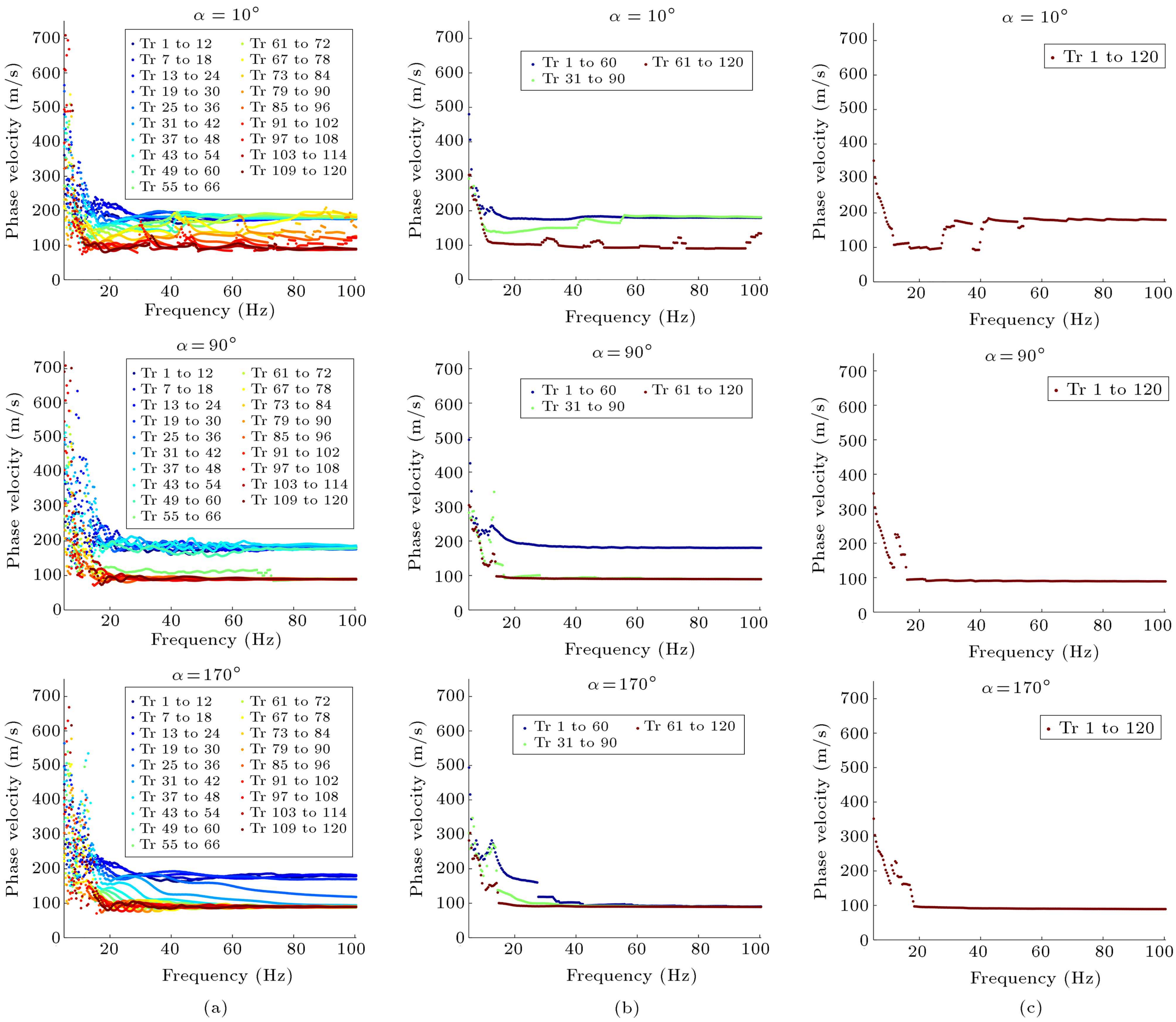

Figure 14. Dispersion curves of the model with a shot on moderate soil and lateral variation of angles 10, 90, and 170 degrees and window length of (a) 12 traces, (b) 60 traces, and (c) 120 traces.

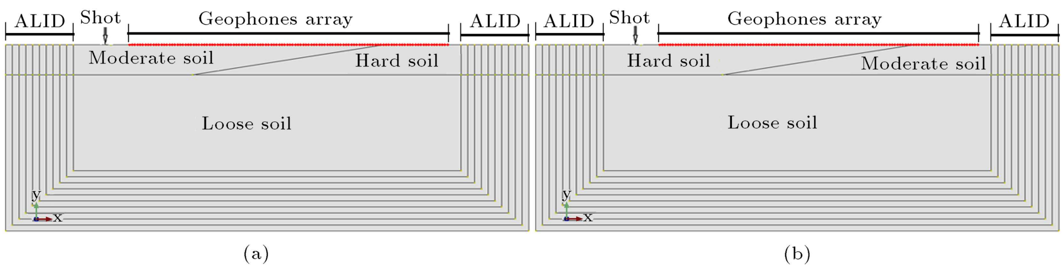

Figure 15. Model of lateral variations with 10-degree angle and shot on moderate soil with reverse velocity (velocity decreases with depth).

variation cause the dispersion curves to be changed (similar to the finding of the previous sections).

5. Conclusion

In this study, the 2D single-layer soil models with lateral variations at different angles were generated on the half-space in ABAQUS finite element software. 120 receivers with the same distances along an array line were used to record the waves. In these models, an active shot on two sides of the array (one in loose soil and another in moderate soil) was used to create the

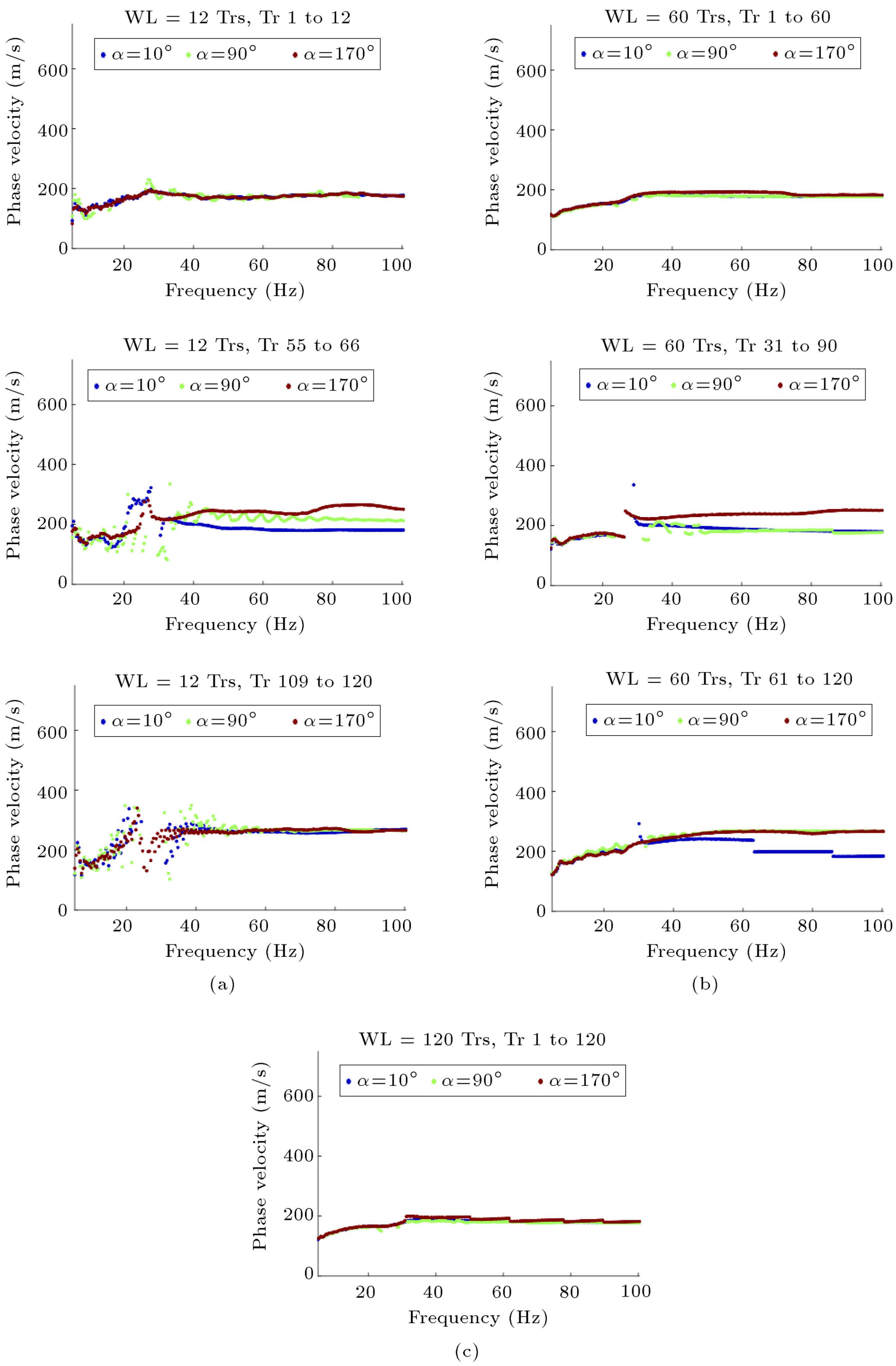

Figure 16. Dispersion curves of models with reverse velocity and shot on moderate soil at different angles of lateral variation for window length of (a) 12 traces, traces 1–12, 55–66 and 109–120, (b) 60 traces, traces 1–60, 31–90 and 61–120, and (c) 120 traces, traces 1–120.

wave field. In the data processing step, the windows of different lengths incorporating the number of different traces (12 to 120 traces with 12-trace increment) were used to determine the effect of the windowing on the determination of dispersion curves. Using the double Fourier transform, the dispersion curves were obtained for each windowing. The results are presented as follows.

In all models, the data related to the traces represents well the location of the lateral variations to the ground surface. In the frequency-wavenumber spectra of different windows, depending on whether in the location of the center of the window near the ground surface, there is a soil with loose or hard properties, the maximum values of the spectrum are achieved along a low slope (for larger wavenumbers,

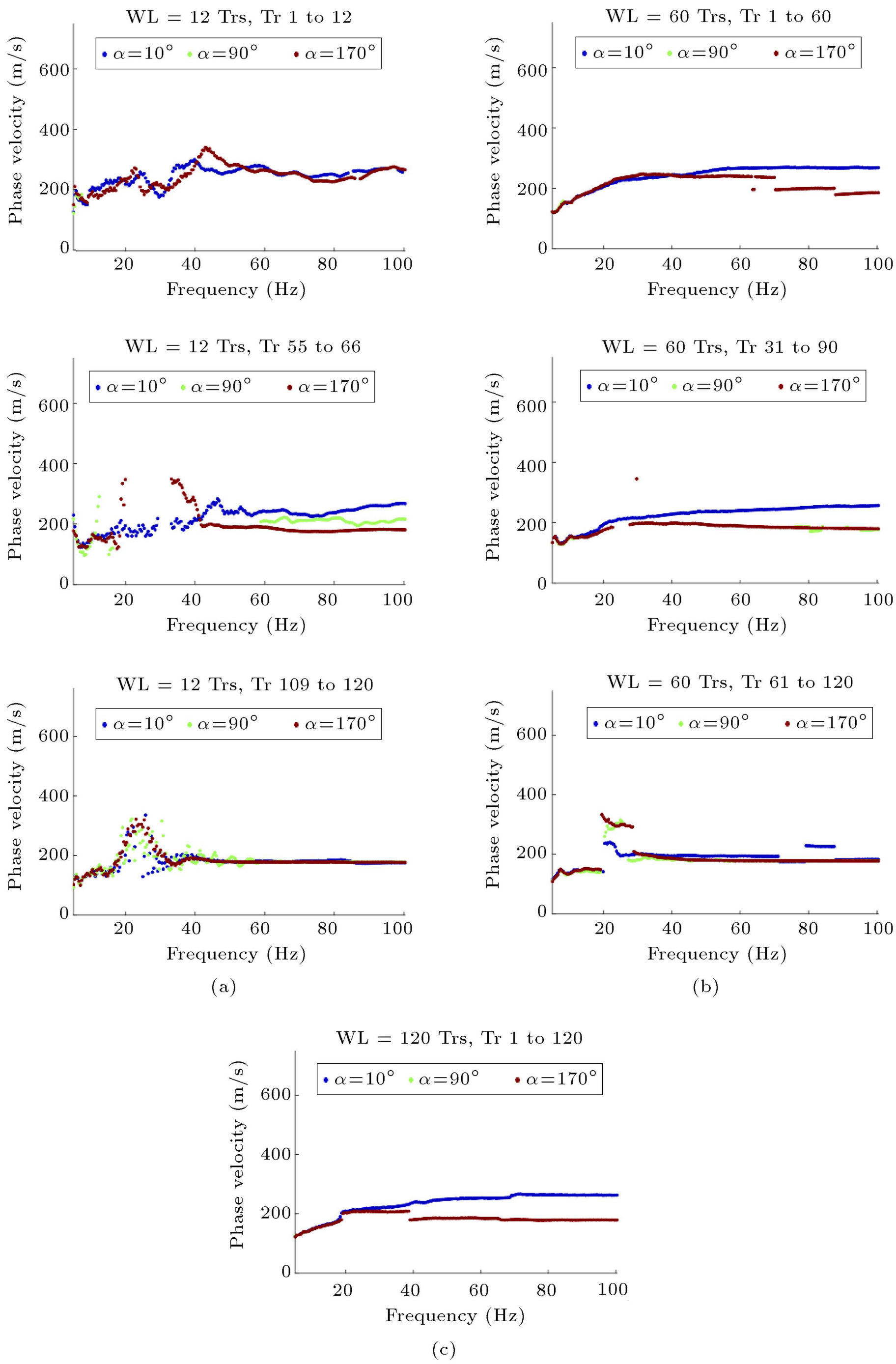

Figure 17. Dispersion curves of models with reverse velocity and shot on hard soil at different angles of lateral variation for window length of (a) 12 traces, traces 1–12, 55–66 and 109–120, (b) 60 traces, traces 1–60, 31–90 and 61–120, and (c) 120 traces, traces 1–120.

lower frequencies) or a sharp slope (for larger wavenumbers, lower frequencies). For small-length windows, the maximum values of the frequency-wavelength spectrum are obtained with lower resolution, and by increasing the length of the window, a higher resolution spectrum could be achieved. For the windowing with a small length, as the window moves along the array, the location of the start and end of the inclined lateral variations inside the ground is obtained. For the windows located before the lateral variations, there will be no special variation between the dispersion curves of the windows. By reaching the location of the start of lateral variations, the dispersion curve is also subjected to changes, and depending on whether the soil becomes looser or harder, the dispersion curve changes to less or more phase velocities, respectively. By passing through the lateral variations, the dispersion curve will fluctuate around the phase velocity of the soil located along the window. Therefore, using the windowing of different length, we will be able to find the start and end location of the lateral variations of any angle with acceptable accuracy, and also we could determine the phase velocity range corresponding to the center of each of the windows from the dispersion curve which can be used in the inversion step and for determining the initial shear wave velocity range. Hence, the shear wave velocity will be achieved along the layout with more appropriate speed and accuracy, which leads to saving the time and cost of specifying the soil properties.

References

1. Strobbia, C., Boaga, J., Cassiani, G., et al. "Integrated seismic characterization for deep engineering targets: active and passive surface waves, reflection and refraction near-surface modelling from a single acquisition", *International Conference on Engineering Geophysics*, Al Ain, United Arab Emirates (2017).
2. Boaga, J., Hashemi Jokar, M., Petronio, L., et al. "Surface waves analysis to detect buried lateral discontinuities: a case study in the trieste port area", Gruppo Nazionale di Geofisica della Terra Solida (GNGTS), 36° convegno nazionale (National Group of Solid Earth Geophysics (GNGTS), 36th national conference), Trieste, Italy (2017).
3. Hashemi Jokar, M. and Mirasi, S. "Using adaptive neuro-fuzzy inference system for modeling unsaturated soils shear strength", *Soft Computing-A Fusion of Foundations, Methodologies and Applications*, **22**(13), pp. 4493–4510 (2018).
4. Hashemi Jokar, M., Khosravi, A., Heidaripanah, A., et al. "Unsaturated soils permeability estimation by adaptive neuro-fuzzy inference system", *Soft Computing*, **33**(16), pp. 6871–6881 (2018).
5. Rahnema, H., Hashemi Jokar, M., and Khabbaz, H. "Predicting the effective stress parameter of unsaturated soils using adaptive neuro-fuzzy inference system", *Scientia Iranica*, **26**(6), pp. 3140–3158 (2018).
6. Socco, L. and Strobbia, C. "Surface-wave method for near-surface characterization: A tutorial", *Near Surface Geophysics,* **2**(4), pp. 165–185 (2004).
7. Strobbia, C., *Surface Wave Methods: Acquisition, Processing and Inversion*, Torino: Politecnico di Torino, Turin, Italy (2003).
8. Hashemi Jokar, M., Rahnema, H., Boaga, J., et al. "Application of surface waves for detecting lateral variations: Buried inclined plane", *Near Surface Geophysics*, **17**(5), pp. 501–531 (2019).
9. Tian, G., Steeples, D.W., Xia, J., et al. "Useful resorting in surface-wave method with the autojuggie", *Geophysics*, **68**(6), pp. 1906–1908 (2003).
10. Bohlen, T., Kugler, S., Klein, G., et al. "1.5 D inversion of lateral variation of Scholte-wave dispersion", *Geophysics*, **69**(2), pp. 330–344 (2004).
11. Hayashi, K. and Suzuki, H. "CMP cross-correlation analysis of multi-channel surface-wave data", *Exploration Geophysics*, **35**(1), pp. 7–13 (2004).
12. Luo, Y., Xia, J., Liu, J., et al. "Generation of a pseudo-2D shear-wave velocity section by inversion of a series of 1D dispersion curves", *Journal of Applied Geophysics*, **64**(3–4), pp. 115–124 (2008).
13. Socco, L.V., Boiero, D., Foti, S., et al. "Laterally constrained inversion of ground roll from seismic reflection records", *Geophysics*, **74**(6), pp. G35–G45 (2009).
14. Vignoli, G. and Cassiani, G. "Identification of lateral discontinuities via multi-offset phase analysis of surface wave data", *Geophysical Prospecting*, **58**(3), pp. 389–413 (2010).
15. Othmani, C., Dahmen, S., Njeh, A., et al. "Investigation of guided waves propagation in orthotropic viscoelastic carbon-epoxy plate by Legendre polynomial method", *Mechanics Research Communications,* **74**, pp. 27–33 (2016).
16. Othmani, C., Takali, F., and Njeh, A. "Theoretical study on the dispersion curves of Lamb waves in piezoelectric-semiconductor sandwich plates GaAs-FGPM-AlAs: Legendre polynomial series expansion", *Superlattices and Microstructures,* **106**, pp. 86–101 (2017).
17. Othmani, C., Njeh, A., and Ghozlen, M.H.B. "Influences of anisotropic fiber-reinforced composite media properties on fundamental guided wave mode behavior: A Legendre polynomial approach", *Aerospace Science and Technology*, **78**, pp. 377–386 (2018).
18. Hashemi Jokar, M., Boaga, J., Petronio, L., et al. "Detection of lateral discontinuities via surface waves analysis: a case study at a derelict industrial site", *Journal of Applied Geophysics*, **164**, pp. 65–74 (2019).
19. Lin, S. "Advancements in active surface wave methods: modeling, testing, and inversion", Ph.D. Thesis, Iowa State University, Ames, Iowa (2014).
20. Lin, S. and Ashlock, J.C. "Surface-wave testing of soil sites using multichannel simulation with one-receiver", *Soil Dynamics and Earthquake Engineering*, **87**, pp. 82–92 (2016).
21. Castaings, M., Bacon, C., Hosten, B., et al. "Finite element predictions for the dynamic response of thermo-viscoelastic material structures", *The Journal of the Acoustical Society of America*, **115**(3), pp. 1125–1133 (2004).
22. Hesse, D. and Cawley, P. "Surface wave modes in rails", *The Journal of the Acoustical Society of America*, **120**(2), pp. 733–740 (2006).
23. Zhu, K. and Fang, D. "Calculation of dispersion curves for arbitrary waveguides using finite element method", *International Journal of Applied Mechanics*, **6**(5), p. 1450059 (2014).
24. ABAQUS v6.14, S., *Abaqus Analysis User's Guide*, Dassault Systémes Simulia Corp., Proidence, RI, USA, www.simulia.com (2014).

25. Drozdz, M.B., *Efficient Finite Element Modelling of Ultrasound Waves in Elastic Media*, Imperial College London (2008).

26. Helwany, S., *Applied Soil Mechanics with ABAQUS Applications*, John Wiley & Sons (2007).

27. Marburg, S. "Discretization requirements: How many elements per wavelength are necessary?", in *Computational Acoustics of Noise Propagation in Fluids-Finite and Boundary Element Methods*, pp. 309–332 (2008).

28. Olivier, G., Brenguier, F., Campillo, M., et al. "Body-wave reconstruction from ambient seismic noise correlations in an underground mine", *Geophysics*, **80**(3), pp. KS11–KS25 (2015).

Biographies

Mehdi Hashemi Jokar received a BS degree in Civil Engineering from Tabriz University and MSc degree in Geotechnical Engineering from Graduate University of Advanced Technology, a first rank student in both degrees. He is currently a PhD candidate in Geotechnical Engineering at Shiraz University of Technology, Shiraz, Iran. He is interested in the determination of the characteristics of soil, especially soft clays, experimental work on the soil, modelling and evaluation of the soil samples, and also design, and site characterization. During his MSc program, he studied the cells that measure soils' characteristics (besides, he worked on his thesis about designing and constructing a cell for determination of soil characteristics such as swelling parameters with different moisture and pressure levels and for determination of the reaction of structures foundation built on expansive soils). He has some experience in designing a cell able to measure soils' characteristics, especially in various moisture and pressure levels. Some part of the cell has been completed; however, it has not been completed yet. He has exclusively studied Fuzzy Logic and Adaptive Neuro-Fuzzy Inference System (ANFIS). He has adopted MATLAB software and has written MATLAB codes that can solve engineering problems relating to the optimum condition of ANFIS. It is possible to predict soil characteristics by ANFIS wrote codes with high accuracy. He is also interested in fabricating a new seismic apparatus and performing field seismic tests with numerical and analytical modelling to investigate his research interests.

Hossein Rahnema is an Assistant Professor in Civil and Environmental Engineering at Shiraz University of Technology. He received all of his educational degrees in Shiraz, Iran. He obtained a PhD in Geotechnical Engineering from Civil Engineering Department of Shiraz University, Shiraz, Iran in 2002. His research field was centered on unsaturated soil. Currently, his primary field of research interest is natural hazards engineering. Within this broad field, he has interests in geotechnical earthquake engineering, including soil-structure interaction and surface wave method as well as seismic hazard analysis, damage detection, and land subsidence. He is interested in fabricating a new seismic apparatus and performing field seismic tests with numerical and analytical modelling to investigate his aforementioned research interests.

Abdolhossein Baghlani is currently the Associate Professor of Civil and Environmental Engineering Department at Shiraz University of Technology, Shiraz, Iran. He received his BS degree in Civil Engineering at Shiraz University, Shiraz, Iran in 1995, his MS degree in Civil Engineering-Hydraulic Structures from Shiraz University in 1998, and his PhD degree in Hydraulic Structures from the same university in 2007. His areas of research and interest are numerical methods in civil engineering, Computational Fluid Dynamics (CFD), fluid-structure interaction, and engineering optimization.